INVESTIGATION OF TWO BODIES WITH EQUAL POINT X-RAYS AT TWO SOURCES

DUSTY ROSS AND KATHLEEN TUITE

ADVISOR: DON SOLMON
OREGON STATE UNIVERSITY

ABSTRACT. We exhibit results that show when there is a possibility for a given body to have a shadow body with the same point X-rays from two sources. We discuss methods for finding the location of the aforementioned shadow body and implement techniques for constructing an approximation of one such shadow body. We show the local existence and convexity of the shadow body at certain points. Finally, we discuss an analytic method of constructing a shadow body and where further investigation of such a method could lead.

1. INTRODUCTION

The subject of tomography deals with examining sets of lower dimensional representations of objects, such as projections or x-rays, where an x-ray function might be what you would typically imagine in terms of medical x-rays. In our situation, it is a simpler function that just records the length of the intersection of all rays emanating from a point source with an object, as if the object were of constant density equal to one. This assumes that there is no fall off related to distance from the source of the x-ray beam, as is the case with real world x-rays.

In our case, we are concerned with 2-dimensional convex bodies existing in the real plane and what information we can deduce about these bodies from x-ray functions (as described above) of these bodies.

It is known that directed x-rays from two sources with the line passing through the sources intersecting the body are enough to uniquely determine the body [6], as are x-rays from three non-co-linear sources [8]. However, in 1983 Falconer posed the question: can there exist more than one body with the same x-ray functions at two sources if the x-ray functions are point x-rays instead of directed x-rays? We have developed some strong evidence that this is, indeed, the case. We have also made heavy use of the computer to visualize our various ideas and propositions to make sure we are headed in the right direction. We have even approximately constructed the shadow body whose existence we are trying to prove. We have also begun to develop a method of analytic construction that could simplify the process of proving existence. It should be noted that we only consider the cases where both sources are outside of the body in question.

Date: 8/17/06.

This work was done during the Summer 2006 REU program in Mathematics at Oregon State University.

2. Definitions and Examples

Definition 2.1. *A **convex body**, K, is a compact, convex subset of the plane with non-empty interior. The boundary of K will be denoted ∂K.*

Definition 2.2. *A body K is **star shaped** at a source P if each ray emanating from P intersects K in a (possibly degenerate) line segment.*

Definition 2.3. *Given a convex body K, a source p, and an angle $\phi \in [0, 2\pi)$, the **nearside point (farside point)** can be defined as the nearest (furthest) point in $r_\phi \cap K$ where r_ϕ is the ray emanating from p that makes angle ϕ with some fixed axis (usually the x-axis).*

Definition 2.4. *The **nearside function**, $r(\phi)$, is defined as the distance to the point on the nearside of the body for each angle ϕ. Similarly, the **farside function**, $R(\phi)$, is defined as the distance to the point on the farside of the body for the same angle ϕ.*

Definition 2.5. *Let p be a point in the plane and let K be a convex body. The **point X-ray of K at P** is a function X_p, defined on $[0, \pi)$, such that for all $\phi \in [0, \pi)$,*

$$X_p(\phi) = \lambda_1(K \cap (l_\phi + p)),$$

where l_ϕ is the line through the origin rotated ϕ radians from the x-axis and λ_1 signifies length.

Definition 2.6. *Let p be a point in the plane and let K be a convex body. The **directed X-ray of K at P** is a function X_p, defined on $[0, 2\pi)$, such that for all $\phi \in [0, 2\pi)$,*

$$X_p(\phi) = \lambda_1(K \cap (r_\phi + p)),$$

where r_ϕ is the ray from the origin rotated ϕ radians from the x-axis and λ_1 signifies length. The directed X-ray can equivalently be defined as $X_p(\phi) = R(\phi) - r(\phi)$.

Note: If it is not clear, it will be noted whether ϕ is measured clockwise or counterclockwise.

Definition 2.7. *Without loss of generality, we can always assume the two x-ray sources to be located on the x-axis. Thus we define the **base line** to be the x-axis of a Cartesian coordinate system, and also the line $\phi = 0$ in polar coordinates.*

Definition 2.8. *For an x-ray function $X(\phi)$ of a body K from a source P, let $\alpha = \inf\{X(\phi) : X(\phi) > 0\}$ and $\beta = \sup\{X(\phi) : X(\phi) > 0\}$. Define the **support lines of K from P** as the lines emanating from P with angle of inclination equal to α and β.*

Definition 2.9. *The **curvature operator**, $\mathscr{K} f$, characterizes the direction of concavity and is defined as*

$$\mathscr{K} f(\phi) = f(\phi)^2 + 2(f'(\phi))^2 - f(\phi) f''(\phi).$$

$\mathscr{K} f$ is defined when f is C^2 at ϕ and is positive (negative) when the graph of f is concave toward (away from) the source at $(f(\phi), \phi)$.

Definition 2.10. *The **signed curvature** of a function f is given by*

$$\kappa_f = \frac{f^2 + 2(f')^2 - f f''}{(f^2 + (f')^2)^{3/2}}.$$

Thus, $\mathscr{K} f = \kappa_f \cdot ((f^2 + (f')^2)^{3/2})$.

The curvature operator is helpful in establishing local convexity of a body, while the signed curvature provides a unique value at any point on a curve, independent of the parametrization of that curve.

Definition 2.11. *Suppose that* $0 < \phi_1 \leq \phi_2 \leq \phi_3 < \pi$ *and* $r_j = r(\phi_j), j = 1,2,3$. *We define the* ***quadratic form*** Q *by*

$$Q(r_1,r_2,r_3) = r_1r_2\sin(\phi_2-\phi_1)+r_2r_3\sin(\phi_3-\phi_2)-r_1r_3\sin(\phi_3-\phi_1)$$

When Q is positive (negative), the points are concave toward (away from) the origin. When $Q = 0$, *the points lie on a straight line.*

Example 2.12. *(We shall refer to this example throughout the rest of the paper.)*

The two sources, P and Q, are located at (0,0) and (10,0).

The original convex body we are dealing with is the lens-shaped intersection of two circles of radius 2 centered at (12,0) and (15,0). Thus, the points a and b on the baseline of this body are (13,0) and (14,0). See Figure 1.

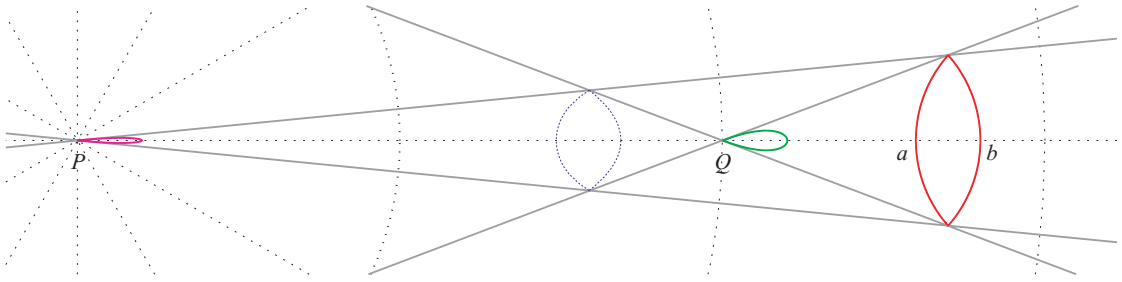

FIGURE 1. Original Body and Sources

The x-ray functions appear as follows (Figure 2), with the wider function representing X_q.

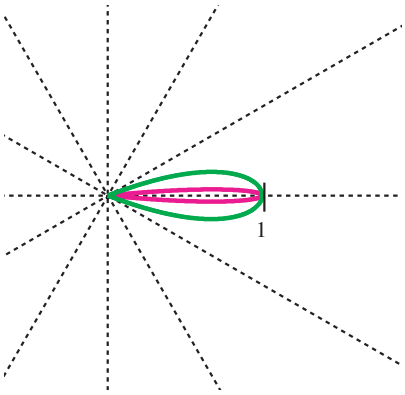

FIGURE 2. X-ray Functions

The x-ray functions are defined for this particular body as follows. They are derived from subtracting the polar equations for two circles between the angles where the circles overlap. From source P, we have

$$X_p(\phi) = \begin{cases} 3\cos(\phi) + 2\sqrt{36\cos^2(\phi) - 35} + \sqrt{225\cos^2(\phi) - 221} & \text{if } |\phi| \leq \alpha \\ 0 & \text{otherwise} \end{cases}$$

where $\alpha = \tan^{-1}(\frac{\sqrt{7}}{27})$. *Then from source Q, we have*

$$X_q(\psi) = \begin{cases} -\cos(\psi) + \sqrt{25\cos^2(\psi) - 21} & \text{if } |\psi| \leq \beta \\ 0 & \text{otherwise} \end{cases}$$

where $\beta = \tan^{-1}(\frac{\sqrt{7}}{7})$.

Note: α and β are the aforementioned support lines.

3. Location of Shadow Body

Given a convex body K in the plane, in order to find a second body with the same point X-rays as K, we first need to examine the possible locations of this shadow body. This problem was simplified in [4]. The important lemma in [4] that pertains to this particular question states the following.

Lemma 3.1. *Let K have point X-ray functions* f_1 *and* f_2 *at P and Q where l, containing P and Q, cuts intK. Let* a, b *be the points of* $l \cap \partial K$. *Writing* p_1, q_1, p_2, q_2 *for the (signed) distances* Pb, Pa, Qb, Qa *respectively, we have*

$$\lim_{\varepsilon \to \infty} \frac{1}{2} \left[\int_{\pi-\varepsilon}^{\varepsilon} \frac{f_2(\phi)}{\sin(\phi)} d\phi - \int_{\pi-\varepsilon}^{\varepsilon} \frac{f_1(\phi)}{\sin(\phi)} d\phi \right] = p_1 \ln|p_1| - p_2 \ln|p_2| - q_1 \ln|q_1| + q_2 \ln|q_2|.$$

We label the value of the equality in the lemma with B. Following Falconer, let $m = f_1(0) = f_2(0) = p_1 - q_1 = p_2 - q_2$ and let A be the distance between our two sources. Then from the previous lemma, given f_1 and f_2, we can determine $F(p_1) - F(p_2)$, where

$$F(t) = t \ln|t| - (t-m) \ln|t-m|.$$

So we are left to investigate the solutions of the nonlinear system of equations

$$p_1 - p_2 = A$$
$$F(p_1) - F(p_2) = B.$$

Substituting and solving for B, we can see that the solutions are of the form $G(p_1) = F(p_1) - F(p_1 - A) = B$. For $A = 10$ and $m = 1$, the plot of $G(t)$ is shown in Figure 3. It is easy to see that for different values of B, there will be zero, one, or two solutions to our system of equations. It is our goal to discover exactly when there are zero, one, or two solutions. Further, we are most interested in the case when there are two solutions, as that will allow the possibility for a convex shadow body.

Further investigation of G leads to the generalization of G for any values A, and m where we have the following.

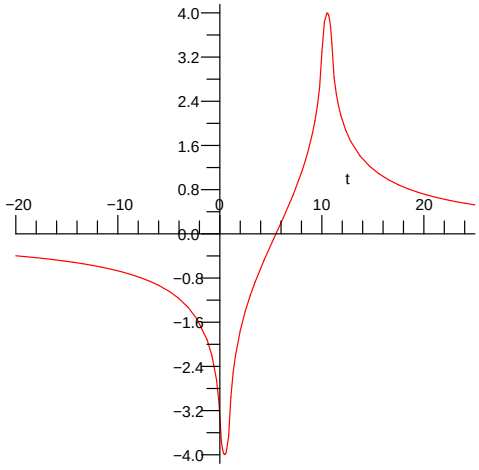

FIGURE 3. Graph of $G(t)$ for $A = 10$ and $m = 1$.

Note: As defined, G is not defined at values 0, m, A, *and* $A+m$. *However, it is easy to see that the limit exists at these points and so for all of our purposes, we will define the function as the limit at these points. Thus, we will consider G to be a continuous function.*

Lemma 3.2. *For any positive values A and m, the function* $G(t)$, *as defined above, possesses the following properties:*

(1) $\lim_{t\to\pm\infty} G(t) = 0$.

(2) *G achieves an absolute minimum at* $t = \frac{1}{2}(A+m-\sqrt{A^2+m^2})$ *and an absolute maximum at* $t = \frac{1}{2}(A+m+\sqrt{A^2+m^2})$. *Further, the maximum value is equal to the negative of the minimum value.*

(3) $G(t) = 0$ *if and only if* $t = \frac{A+m}{2}$. *That is, if and only if the given body is centered with respect to the two sources. Thus, there is a unique solution to the system of equations when the body is centered.*

Proof. The lemma can be proved using basic Analysis and Differential Calculus.

(1) Notice that

$$G(t) = t\ln|t| - (t-m)\ln|t-m| - (t-A)\ln|t-A| + (t-(A+m))\ln|t-(A+m)|.$$

By distributing and using properties of logarithms, we can rewrite this as

$$G(t) = t\ln\left|\frac{t^2-t(A+m)}{t^2-t(A+m)+Am}\right| + m\ln\left|\frac{t-m}{t-(A+m)}\right| + A\ln\left|\frac{t-A}{t-(A+m)}\right|.$$

In all three terms, the numerator and denominator embedded in the logarithm only differ by a constant. Thus as $t \to \pm\infty$, all three terms converge to 0.

(2) Computing the derivative of G, we get

$$G'(t) = \ln|t| - \ln|t-m| - \ln|t-A| + \ln|t-(A+m)|.$$

Using properties of logarithms, we can rewrite this as

$$G'(t) = \ln\left|\frac{t^2 - t(A+m)}{t^2 - t(A+m) + Am}\right|.$$

Using properties of the natural log, one can see that G will be increasing when $|t^2 - t(A+m)| > |t^2 - t(A+m) + Am|$, decreasing when $|t^2 - t(A+m)| < |t^2 - t(A+m) + Am|$, and it will have a horizontal tangent when $|t^2 - t(A+m)| = |t^2 - t(A+m) + Am|$. Observing that $t^2 - t(A+m) + Am$ is a positive translation of the parabola $t^2 - t(A+m)$, we know that the absolute values of the two will only be equal if the first is positive and the second is negative (see figure). Thus, we get the equation $t^2 - t(A+m) + Am = -t^2 + t(A+m)$. Applying the quadratic formula, we get the desired result in order for $G'(t) = 0$. It is easy to check that the maximum is the negative of the minimum.

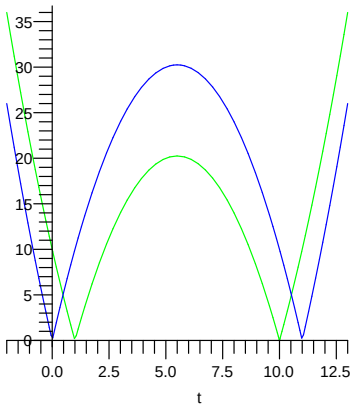

FIGURE 4. Graph of $|t^2 - t(A+m)|$ and $|t^2 - t(A+m) + Am|$ for $A = 10$ and $m = 1$.

Observing the behavior of the absolute value of quadratic functions, it is clear that $G'(t) < 0$ for all $t < \frac{1}{2}(A+m-\sqrt{A^2+m^2})$ and $t > \frac{1}{2}(A+m+\sqrt{A^2+m^2})$. Similarly, $G'(t) > 0$ for $\frac{1}{2}(A+m-\sqrt{A^2+m^2}) < t < \frac{1}{2}(A+m+\sqrt{A^2+m^2})$. Thus, G obtains a max and min at the points stated in the lemma.

(3) This is a direct consequence of the previous comments and part (1) of the lemma.

□

The results of the previous lemma lead us to the next theorem.

Theorem 3.3. *Given positive values of A and m, the function G will have no solutions when* $|B| > G\left(\frac{1}{2}(A+m+\sqrt{A^2+m^2})\right)$*, one solution if* $|B| = G\left(\frac{1}{2}(A+m+\sqrt{A^2+m^2})\right)$ *or* $B = 0$*, and two solutions for every other B value.*

This theorem can be used as a consistency requirement that must be satisfied in order for two functions defined at two points to be point X-rays of a planar convex body. We have the following.

Theorem 3.4. *Suppose f_1 and f_2 are two functions defined on $[0,\pi)$ at points P and Q. Without loss of generality, we can assume that P and Q are on the x-axis. Suppose that $f_1(0) = f_2(0) = m > 0$. Let $A = |P-Q|$. Let*

$$B = \lim_{\varepsilon\to\infty} \frac{1}{2}\left[\int_{\pi-\varepsilon}^{\varepsilon} \frac{f_2(\phi)}{\sin(\phi)}d\phi - \int_{\pi-\varepsilon}^{\varepsilon} \frac{f_1(\phi)}{\sin(\phi)}d\phi\right].$$

If f_1 and f_2 are point X-rays of a convex planar body, then

$$|B| \le G\left(\frac{1}{2}(A+m+\sqrt{A^2+m^2})\right).$$

Proof. This theorem is a direct consequence of the previous theorem. If $|B| > G\left(\frac{1}{2}(A+m+\sqrt{A^2+m^2})\right)$, then there are no solutions to the system of equations. □

The previous theorem is most helpful in the form of its contrapositive. If two equations fit the hypothesis but do not satisfy the inequality, then one can be sure that they are not point X-rays of a convex planar body.

Although solving explicitly for solutions of G is beyond our scope, it is possible to use Maple to find approximations of ten decimal places (or more) for second solutions. This will prove helpful in constructing computer generated approximations of a shadow body as it will give us a starting point to begin the construction algorithm. It is also useful in proving local convexity properties near the baseline.

In Example 2.12 we used the original value of $p_1 = 14$ to find $B = 1.35312$. We then plotted G and the line $y = B$ to approximate points of intersection. Using the fsolve command of Maple, we searched for a second solution near $t = 8$ and found the second $p_1 = 8.43126$. See Figure 5. Thus if there is a shadow body, it will intersect the baseline at approximately 7.43126 and 8.43126.

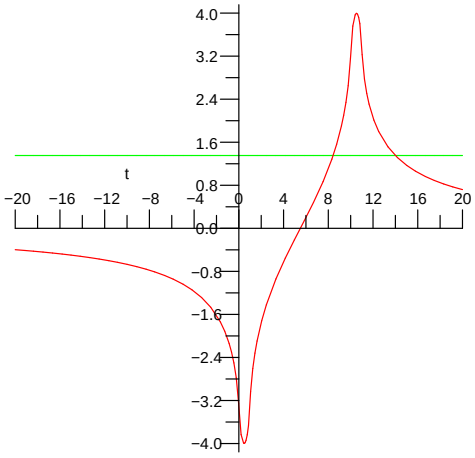

FIGURE 5. Graphs of G and $y = B$.

4. Approximate Construction of the Shadow Body

Solving the system of nonlinear equations from the previous section using the position of our original body and sources gives us the position of our shadow body at the baseline. The points where it intersects the baseline are at 7.43126 and 8.43126. At this point, it seems like a good idea to try to construct this body even though we are unsure of its existence. The results are encouraging:

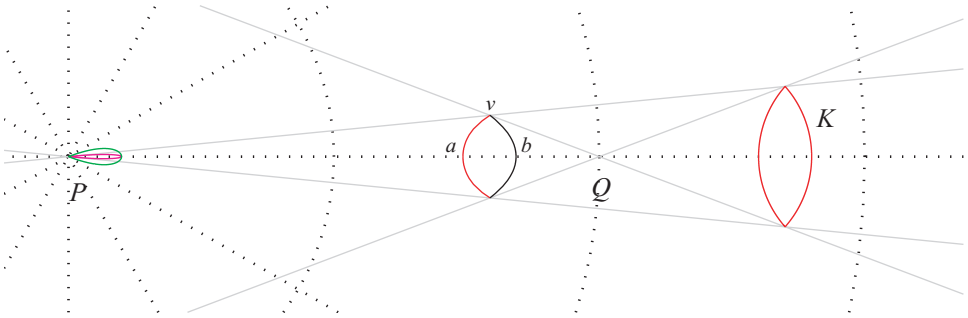

FIGURE 6. Reconstructed Shadow Body (center) and Original Body K.

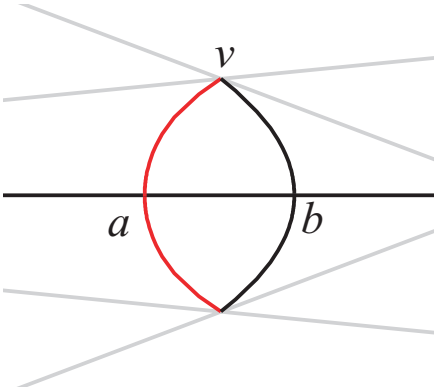

FIGURE 7. Shadow Body with Points $a = (7.4313, 0), b = (8.4313, 0), v = (7.9412, 0.7782)$

4.1. **Construction From the Base Line.** An algorithm for construction was first suggested by Dartmann [2]. If one takes the body being constructed to be in between the two sources, the process of construction involves approximating a small portion of the body near the baseline, adding the x-ray data from one source to that small portion to get a larger portion of the body on the other side, and then repeating the process from the other source. It is possible to build up the entire body this way, by pushing up the edge of the body back and forth from each source, a process called 'chord chasing'. When Dartmann did his construction, he approximated the body at the baseline with a vertical tangent line. Seifken and Spargo [7] came up with a way to find more accurate tangent lines at the base points. However, since the body we are using is symmetric over the x-axis and smooth in a neighborhood of the x-axis, the tangent lines at the baseline are vertical.

Since our original body is lens-shaped and far enough away from the sources, the support rays from the two sources intersect each other at the top and bottom vertices of the body. This means that the other intersections of the support rays will be the top and bottom vertices of the shadow body. Were this not the case, if the support rays did not touch the body at the very top, we would not be able to use this method of construction. See Figure 8. Point v is on the far side with respect to both P and Q so it is no longer possible to add x-ray data from Q. Subtracting x-ray data is the only option to get back to a point on the body, but that does not lead to any more progress with the construction.

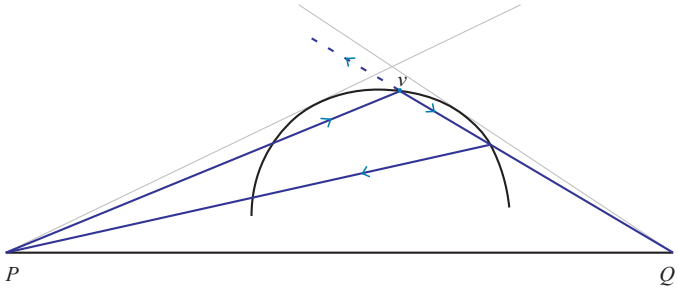

FIGURE 8. Problems with Construction for a Smooth Topped Body

We could construct both the original body and the shadow body using the following algorithms, but we are going to focus on building the shadow body. It has the same point x-rays as the original body, so all that is needed additionally is some information about its location, which we found in the previous section. We will start by using the body's position on the baseline to build upwards.

Algorithm 1 requires that the body being constructed be symmetric over the x-axis and located between the two sources. When constructing a shadow body, this means that the original body is outside the sources.

Some comments on the algorithm:

- A smaller *initialAngle* yields a more accurate approximation.
- The smaller *initialAngle*, the greater *numIterations* will have to be to build all the way to the top.
- Due to approximation errors, the construction will probably not hit the vertex exactly, but veer off to the side and hit a support line when it gets close. If *numIterations* is large enough, the algorithm will keep constructing past the support lines.
- If *numIterations* is too large, too many iterations of the function will force points to cluster near the top of the body; If it smaller, or if *initialAngle* is decreased, points will be more evenly distributed along the edge of the body.
- Store points as ϕ, r_p, R_p, where $R_p = r_p + X_p(\phi)$
- This construction only builds the upper half of the body. It is clear that the lower half is simply the reflection over the x-axis.

Since it is impossible to exactly evaluate location of the base points using results from Section 3, and also for the computer to go beyond a certain degree of accuracy, the construction algorithm

Algorithm 1 Construction From the Bottom Up

procedure BOTTOM-UP-CONSTRUCTION
  $P \leftarrow$ location of first source
  $Q \leftarrow$ location of second source
  Define x-ray functions $X_p(\phi)$ and $X_q(\phi)$
  Find angle of left tangent line at vertex.
  $leftBasePoint \leftarrow$ left point on baseline of body being reconstructed.
  $initialAngle \leftarrow$ some small angle
  $numIterations \leftarrow$ number of times to iterate each point
  Build an array of n points along tangent line between angles 0 and $initialAngle$.
  for i = 1, $numIterations$ **do**
    for all n points (ϕ, r_p, R_p) **do**
      $r_q \leftarrow \sqrt{R_p^2 + (Q-P)^2 - 2R_p(Q-P)\cos\phi}$
      $\psi \leftarrow \sin^{-1}(\frac{\sin(\phi)\cdot R_p}{r_q})$
      $R_q \leftarrow r_q + X_q(\psi)$
      $r'_p \leftarrow \sqrt{R_q^2 + (Q-P)^2 - 2R_q(Q-P)\cos\psi}$
      $\phi' \leftarrow \sin^{-1}(\frac{\sin(\psi)\cdot R_q}{r'_p})$
      Update point with new values $(\phi', r'_p, r'_p + X_p(\phi'))$.
    end for
  end for
  Plot points.
end procedure

is incapable of completing the top of the shadow body. We will, however, prove local existence at the top in the following section. Using Matlab to zoom in on the construction, we see that the top of the shadow body curves off to the side. Perturbing the point on the baseline that we start from causes the wave shape on the top of the body to curl different amounts, and even to the opposite direction. See Figure 9 for an example of what can happen very near the top of a construction, viewed in very fine detail. In this example, there are 200 points, 33 iterations, and an initial angle of $5 \cdot 10^{-9}$ radians. The different values for the left base point are 7.430, 7.431, 7.4312, 7.4313, and 7.4345. The real basepoint is about 7.43126. The fact that the curl changes direction past a certain point suggests that if we were able to have exact calculations, the construction might converge to the intersection of the support rays as expected.

4.2. **Construction From the Top Down.** Since the shadow body we are using has the property that the top vertex is exactly where the support rays intersect, we actually know four points of the body: the two on the baseline and the top and bottom vertices. Because of this, we can use the chord-chasing that we use to construct from the baseline up to construct from the top vertex down toward the baseline. It should even match up with the bottom-up construction if the shadow body is actually to exist.

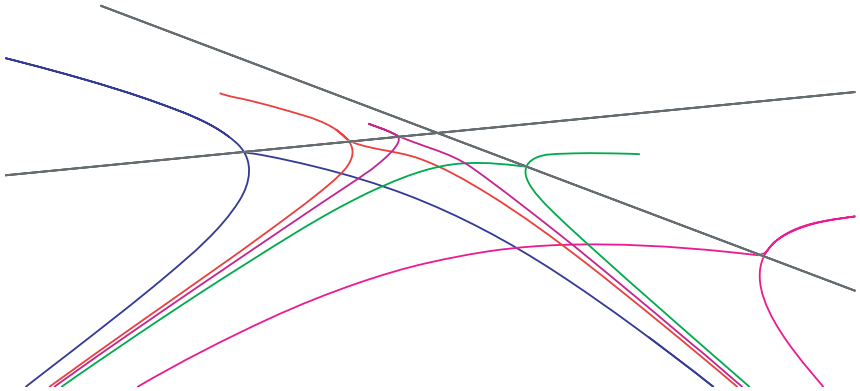

FIGURE 9. Construction Errors

4.2.1. *Tangent Lines at Vertex.* Just as Seifken and Spargo [7] calculated the tangent lines at the baseline, we can compute the tangent lines at the top of the shadow body. Consider the upper part of a body with differentiable x-ray functions defined as $X_p(\phi)$ and $X_q(\psi)$ for $0 \leq \phi \leq \phi_{max}$ and $0 \leq \psi \leq \psi_{max}$ where ϕ_{max} are ψ_{max} the angles of the support rays from sources P and Q. Suppose this body has a vertex at the intersection of the support rays, that is $X_p(\phi_{max}) = X_q(\psi_{max}) = 0$. For notation purposes let $X'_p = X'_p(\phi_{max})$, $X'_q = X'_q(\psi_{max})$, $\phi = \phi_{max}$, and $\psi = \psi_{max}$. Let $t = tan(\phi + \psi)$.

Theorem 4.1. *The angle of inclination for the left tangent line, η_ϕ, can be found by solving the following quadratic equation for* $\cot(\eta_\phi - \phi)$ *and then solving for η_ϕ.*

Note: ψ, η_ψ and ω_ψ are all measured clockwise from the x-axis.

$$\begin{aligned} 0 &= \cot(\eta_\phi - \phi)^2 \cdot \left[t^2 \cdot \frac{r_p}{r_q} \cdot X'_q \right] \\ &\quad + \cot(\eta_\phi - \phi) \cdot \left[2t \cdot X'_p + 2t \cdot \frac{r_p}{r_q} \cdot X'_q - \frac{X'_p \cdot X'_q}{r'_q} \cdot t^2 \right] \\ &\quad + X'_q(1 - t^2) + \frac{r_p}{r_q} \cdot X'_q - \frac{X'_p \cdot X'_q \cdot t}{r_q} \end{aligned}$$

The angle of inclination for the right tangent line, ω_ϕ, can be found using η_ϕ and the following equation.

$$\cot(\omega_\phi - \psi) = \cot(\eta_\phi - \psi) - \frac{X'_p}{r_p}$$

Proof. We shall call the angles of the nearside and farside tangent lines with respect to source P η_ϕ and ω_ϕ. The nearside and farside tangent lines from source Q we shall call η_ψ and ω_ψ. See Figure 10. There is only one point we are considering here, the top vertex of the body, at which there are two tangent lines we wish to find, but we have two angles to look at this point from: ϕ and ψ from sources P and Q. From this we get the relations:

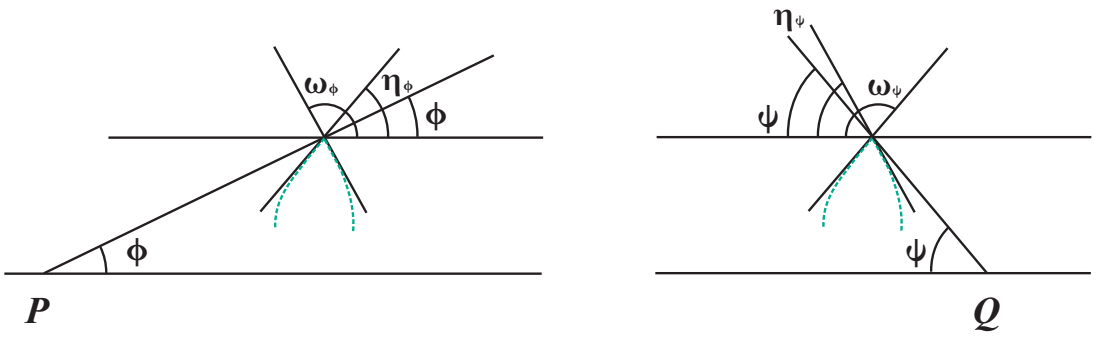

FIGURE 10. Tangent Lines and Angles of Inclination

$$\eta_\phi = \pi - \omega_\psi$$
$$\omega_\phi = \pi - \eta_\psi$$

We also have the following equations from [1] (and a second pair for the other source Q) relating tangent line angles to the nearside and farside functions of the body itself:

$$\frac{r'_\phi}{r_\phi} = \cot(\eta_\phi - \phi)$$
$$\frac{R'_\phi}{R_\phi} = \cot(\omega_\phi - \phi)$$

Since we know that $X_p(\phi) = R_p(\phi) - r_p(\phi)$ and $X'_p(\phi) = R'_p(\phi) - r'_p(\phi)$, and that at the top of the body the nearside and farside points are the same, we can multiply the two equations above by $r_p(\phi)$ on both sides and get the equation

$$X'_p(\phi) = r_p(\phi)\cot(\omega_\phi - \phi) - r_p(\phi)\cot(\eta\phi - \phi) \tag{1}$$

By a similar process, we can also get an equation for $X'_q(\psi)$, but it is useful to replace all instances of η_ψ and ω_ψ with $(\pi - \omega_\phi)$ and $(\pi - \eta_\psi)$. Then we have

$$X'_q(\psi) = r_q(\psi)\cot(\omega_\phi + \psi) - r_q(\psi)\cot(\eta_\phi + \psi) \tag{2}$$

Now the goal is to get rid of ψ and ω_ϕ from equations (1) and (2) and use them together to solve for η_ϕ. Consider the following equations:

$$\cot(\eta_\phi + \psi) = \frac{1 - \tan(\eta_\phi - \psi) \cdot \tan(\phi + \psi)}{\tan(\eta_\phi - \psi) + \tan(\phi + \psi)} \tag{3}$$

$$\cot(\omega_\phi + \psi) = \frac{1 - \tan(\omega_\phi - \psi) \cdot \tan(\phi + \psi)}{\tan(\omega_\phi - \psi) + \tan(\phi + \psi)} \tag{4}$$

$$\tan(\omega_\phi - \psi) = \frac{r_p(\phi)}{r_p(\phi)\cot(\omega_\phi - \phi) + X_p'(\phi)} \tag{5}$$

Equation (5) comes from (1). If we embed (3) into the first operand of (2), and then (5) into (4) and let that replace the second operand of (2), after a bit of rearranging, we get the quadratic equation already mentioned in Theorem 4.1. This quadratic allows us to solve for the nearside tangent line with respect to source P and then it is then easy to see how to use (1) to find the farside tangent line. □

In our example, the slopes of the left and right tangent lines are computed to be -0.79923 and 0.62250.

4.2.2. *Algorithm for Top-Down Construction.* This algorithm (Algorithm 2) is very similar to Algorithm 1. One must find the point of intersection of the support rays and then define n points in a small neighborhood on the left side tangent line at that point. Then the construction procedure goes as follows.

Some comments on the algorithm:

- Remember that α and β are the angles of the support lines from sources P and Q.
- Again, a smaller initial neighborhood means a more accurate approximation.
- If *numIterations* is too large, all the points will converge to points on the baseline, the same points computed with as the shadow body's base points, in fact.
- This construction never actually reaches the baseline. It would take an infinite number of iterations to do so, and one of our main concerns with proving the existence of this shadow body is whether or not there is nasty behavior as we approach the baseline.

The first figure in this section, Figure 6, is made using the top-down construction. The left and right tangent lines have slopes of -0.79923 and 0.62250, respectively. The top-down construction matches up with its bottom-up counterpart quite nicely, to at least 5 significant figures. See Figure 11.

5. Stable Manifold Theorem and Local Existence of Shadow Body

Following Falconer [3], a key method in determining the existence of a shadow body is the Stable Manifold Theorem. It is stated as follows.

Theorem 5.1. *Let $k \geq 1$, $U \subset \mathbb{R}^2$ with U open, $f : U \to \mathbb{R}^2$, a C^k function with $k \geq 2$ and v a fixed point of f. Suppose that the eigenvalues of the differential $df(v)$ are μ, λ with $|\mu| < 1$ and*

Algorithm 2 Construction From the Top Down

procedure TOP-DOWN-CONSTRUCTION
  $P \leftarrow$ location of first source
  $Q \leftarrow$ location of second source
  Define x-ray functions $X_p(\phi)$ and $X_q(\phi)$
  $topVertex \leftarrow$ intersection of support lines.
  $initialAngle \leftarrow$ some small angle
  $numIterations \leftarrow$ number of times to iterate each point
  Build an array of n points along tangent line between angles $\alpha - initialAngle$ and α.
  for i = 1, $numIterations$ **do**
    for all n points (ϕ, r_p, R_p) **do**
      $R_q \leftarrow \sqrt{r_p^2 + (Q-P)^2 - 2r_p(Q-P)\cos\phi}$
      $\psi \leftarrow \sin^{-1}(\sin(\phi)\frac{r_p}{R_q})$
      $r_q \leftarrow R_q$ - $X_q(\psi)$
      $R'_p \leftarrow \sqrt{r_q^2 + (Q-P)^2 - 2r_q(Q-P)\cos\psi}$
      $\phi' \leftarrow \sin^{-1}(\sin(\psi)\frac{r_q}{R'_p})$
      Update point with new values $(\phi', R'_p - X_p(\phi'), R'_p)$
    end for
  end for
  Plot points.
end procedure

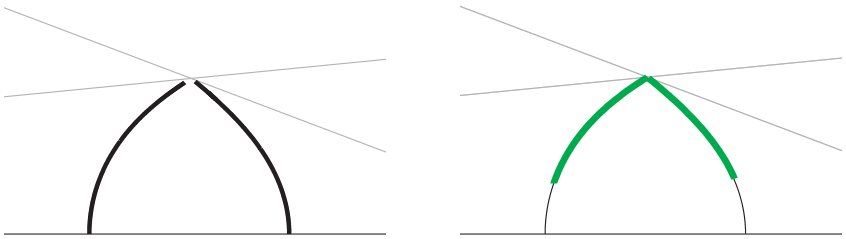

FIGURE 11. Bottom Up and Top Down Constructions Matching Up

$|\lambda| > 1$. *Let E^s, E^u be the eigenspace corresponding to μ, λ, respectively. Then there is some neighborhood U' of v, $U' \subset U$ so that the local stable manifold for v in U',*

$$W^s(v,U',f) = \{x \in U' : f^j(x) \in U'\} = \{x \in U' : f^j(x) \to v \text{ as } j \to \infty\}$$

is a C^k curve which is tangent to E^s. (Here f^j denotes the j-fold composition of f with itself.) More precisely, U' may be chosen so that in U' the stable manifold has the form

$$W^s(v,U',f) = \{v + tu_\mu + s(t)u_\lambda, -r < t < r\}$$

where u_μ and u_λ are unit eigenvectors corresponding to the eigenvalues μ and λ, respectively and $s = s(t)$ is a C^k function satisfying $s(0) = s'(0) = 0$.

We proceed to apply the Stable Manifold Theorem. Let P and Q be the two sources for our X-rays. In our particular situation, we know that we can locate the top vertex in our shadow body, v, because it is precisely where the support lines meet. We will define a function, f, as follows.

In polar coordinates centered at P, let

$$F_1(r,\phi) = (r + X_p(\phi), \phi).$$

Converting this to rectangular coordinates centered at P, we have

$$F_1(x,y) = ((r + X_p(\phi))\cos\phi, (r + X_p(\phi))\sin\phi).$$

In polar coordinates centered at Q, let

$$F_2(s,\psi) = (s + X_q(\psi), \psi).$$

Converting this to rectangular coordinates centered at P, we get

$$F_2(x,y) = (10 - (s + X_q(\psi))\cos\psi, (s + X_q(\psi))\sin\psi).$$

Finally, let $f = F_2 \circ F_1$. See Figure 12.

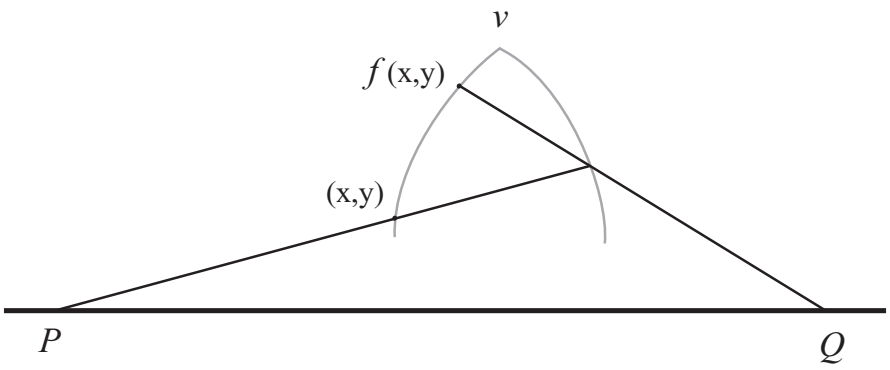

FIGURE 12. The function f that maps points on the body to new points on the body closer to the vertex.

Analytically, we can see that the function f is simply adding X-ray data from source P onto a point in the plane, and then adding the respective X-ray data from Q onto the image. It's clear that, given a point (x,y) on the shadow body, $f^j(x,y) \to v$ as $j \to \infty$. It is also easy to see that the v is a fixed point of f. Using the Chain Rule, we can find the differential of f as follows. For each $i, j \in \{1,2\}$,

$$\frac{\partial f_i}{\partial x_j} = \frac{\partial f_i}{\partial s}\frac{\partial s}{\partial r}\frac{\partial r}{\partial x_j} + \frac{\partial f_i}{\partial s}\frac{\partial s}{\partial \phi}\frac{\partial \phi}{\partial x_j} + \frac{\partial f_i}{\partial \psi}\frac{\partial \psi}{\partial r}\frac{\partial r}{\partial x_j} + \frac{\partial f_i}{\partial \psi}\frac{\partial \psi}{\partial \phi}\frac{\partial \phi}{\partial x_j}.$$

The differential is simply the 2×2 matrix with the partial derivatives as its entries:

$$\begin{pmatrix} \frac{\partial f_1}{\partial x} & \frac{\partial f_1}{\partial y} \\ \frac{\partial f_2}{\partial x} & \frac{\partial f_2}{\partial y} \end{pmatrix}$$

Once the differential is found, it is then possible to solve for the eigenvalues and eigenvectors. We did this using our specific body and the function f and achieved eigenvalues of 4.062 and 0.246. The eigenvector corresponding to the smaller eigenvalue had slope 0.6225. Using previous results, it is possible to compute the slope of r_p at v and so we did this and it agreed with the slope of the eigenvector up to 6 significant figures. Thus, by the Stable Manifold Theorem, we have found local existence of the shadow body at the point v and we know the slope of the tangent line to r_p at the top vertex. We also computed the same results on the other side by using the function $g = F_1 \circ F_2$. This gave us the same eigenvalues but with a slope of -0.79923, which agrees with the previously computed tangent line slope.

Utilizing the functions f^{-1} and g^{-1} we can follow a similar procedure to find local existence at the baseline. One of the eigenvalues of the differential will be equal to 1 so the traditional Stable Manifold Theorem will not apply. Falconer [3] showed, however, that a modified version of the Stable Manifold Theorem can be used in order to get the desired existence at the baseline.

5.1. **General Existence.** We can use a similar approach to show that the Stable Manifold Theorem guarantees existence in the general case where we have two chord functions that vanish at a fixed point v where the x-coordinate of v is between the two sources. Let X_p and X_q be two chord functions at $(P,0)$ and $(Q,0)$, respectively, so that $v = (x_0, y_0)$ is a point at which both chord functions vanish. Also, we require that the x coordinate of v is greater than P and less than Q. Let $A = Q - P$. We can define f as follows:
In rectangular coordinates, let

$$F_1(x,y) = (x + X_p(\phi)\cos(\phi), y + X_p(\phi)\sin(\phi))$$

where

$$\tan(\phi) = y/x.$$

Similarly, let

$$F_2(x,y) = (x - X_q(\psi)\cos(\psi), y + X_q(\psi)\sin(\psi))$$

where

$$\tan(\psi) = y/(A - x).$$

Now let $f = F_2 \circ F_1$. It should be clear that f is the same function that we defined above. We can now computer the differentials of F_1 and F_2 at v. We will refer to F_{ij} as the jth component of F_i for $i, j \in \{1,2\}$. Let $r_\alpha = d(P,v)$, $s_\beta = d(Q,v)$ (α and β here are analogous to the angle of inclination of our support lines discussed earlier). Let $L_p = x_0 - P$ and $L_q = A - x_0$. Let $h = y_0$. See Figure 13 Noticing that $\sin(\alpha) = \frac{h}{r_\alpha}$, $\cos(\alpha) = \frac{L_p}{r_\alpha}$, $\frac{\partial \phi}{\partial x}(v) = \frac{-h}{r_\alpha^2}$, and $\frac{\partial \phi}{\partial y}(v) = \frac{L_p}{r_\alpha^2}$ we can see that

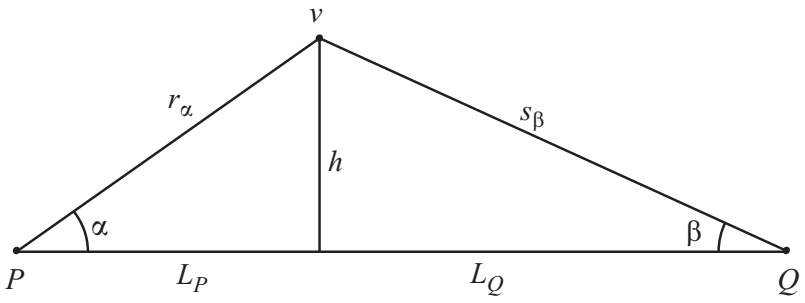

FIGURE 13. Labels for General Existence

$$\frac{\partial F_{11}}{\partial x}(v) = 1 + X_p'(\alpha)\cos(\alpha)\frac{\partial \phi}{\partial x}(v) = 1 - X_p'(\alpha)\frac{L_p h}{r_\alpha^3},$$
$$\frac{\partial F_{11}}{\partial y}(v) = X_p'(\alpha)\cos(\alpha)\frac{\partial \phi}{\partial y}(v) = X_p'(\alpha)\frac{L_p^2}{r_\alpha^3},$$
$$\frac{\partial F_{12}}{\partial x}(v) = X_p'(\alpha)\sin(\alpha)\frac{\partial \phi}{\partial x}(v) = -X_p'(\alpha)\frac{h^2}{r_\alpha^3}, \text{ and}$$
$$\frac{\partial F_{12}}{\partial y}(v) = 1 + X_p'(\alpha)\sin(\alpha)\frac{\partial \phi}{\partial y}(v) = 1 + X_p'(\alpha)\frac{L_p h}{r_\alpha^3}.$$

We can then compute the Jacobian Matrix of F_1 to be

$$dF_1(v) = \begin{pmatrix} 1 - X_p'(\alpha)\frac{L_p h}{r_\alpha^3} & X_p'(\alpha)\frac{L_p^2}{r_\alpha^3} \\ -X_p'(\alpha)\frac{h^2}{r_\alpha^3} & 1 + X_p'(\alpha)\frac{L_p h}{r_\alpha^3} \end{pmatrix}$$

from which it should be clear that the determinant, $|dF_1|$, is equal to 1.

Similarly, noticing that $\sin(\beta) = \frac{h}{s_\beta}$, $\cos(\beta) = \frac{L_q}{s_\beta}$, $\frac{\partial \psi}{\partial x}(v) = \frac{h}{s_\beta^2}$, and $\frac{\partial \psi}{\partial y}(v) = \frac{L_q}{s_\beta^2}$ we can see that

$$\frac{\partial F_{21}}{\partial x}(v) = 1 - X_q'(\beta)\cos(\beta)\frac{\partial \psi}{\partial x}(v) = 1 - X_q'(\beta)\frac{L_q h}{s_\beta^3},$$
$$\frac{\partial F_{21}}{\partial y}(v) = -X_q'(\beta)\cos(\beta)\frac{\partial \psi}{\partial y}(v) = -X_q'(\beta)\frac{L_q^2}{s_\beta^3},$$
$$\frac{\partial F_{22}}{\partial x}(v) = X_q'(\beta)\sin(\beta)\frac{\partial \psi}{\partial x}(v) = X_q'(\beta)\frac{h^2}{s_\beta^3}, \text{ and}$$
$$\frac{\partial F_{22}}{\partial y}(v) = 1 + X_q'(\beta)\sin(\beta)\frac{\partial \psi}{\partial y}(v) = 1 + X_q'(\beta)\frac{L_q h}{s_\beta^3}.$$

We can now compute the Jacobian Matrix F_2 to be

$$dF_2(v) = \begin{pmatrix} 1 - X_q'(\beta)\frac{L_q h}{s_\beta^3} & -X_q'(\beta)\frac{L_q^2}{s_\beta^3} \\ X_q'(\beta)\frac{h^2}{s_\beta^3} & 1 + X_q'(\beta)\frac{L_q h}{s_\beta^3} \end{pmatrix}$$

from which it should be apparent that $|dF_2| = 1$. Since v is a fixed point for both F_1 and F_2, we know that

$$df(v) = dF_2(v) \cdot dF_1(v) = \begin{pmatrix} 1 - X_q'(\beta)\frac{L_q h}{s_\beta^3} & -X_q'(\beta)\frac{L_q^2}{s_\beta^3} \\ X_q'(\beta)\frac{h^2}{s_\beta^3} & 1 + X_q'(\beta)\frac{L_q h}{s_\beta^3} \end{pmatrix} \cdot \begin{pmatrix} 1 - X_p'(\alpha)\frac{L_p h}{r_\alpha^3} & X_p'(\alpha)\frac{L_p^2}{r_\alpha^3} \\ -X_p'(\alpha)\frac{h^2}{r_\alpha^3} & 1 + X_p'(\alpha)\frac{L_p h}{r_\alpha^3} \end{pmatrix}.$$

Thus, $|df(v)| = |dF_2(v)| \cdot |dF_1(v)| = 1$.

This approach also gives us a method to compute the Jacobian of the function f at v. It suffices to find each Jacobian Matrix at F_1 and F_2 using the formulas given above, and then multiplying them together. One can then solve for the eigenvalues and eigenvectors explicitly.

The trace (sum of diagonal entries) of the Jacobian Matrix can also be used to compute the eigenvalues and subsequent eigenvectors. Noticing that the characteristic polynomial of a 2×2 matrix A is equivalent to $\lambda^2 - tr(A)\lambda + \det(A) = 0$, we can see that the eigenvalues of A are uniquely determined by the trace and determinant. Further, applying the quadratic formula, we see that

$$\lambda = \frac{tr(A) \pm \sqrt{tr(A)^2 - 4\det(A)}}{2}.$$

Since we know that $\det(df(v)) = 1$, we just need to compute $tr(df(v))$. Since $df(v) = dF_2(v) \cdot dF_1(v)$, we can compute the trace of $df(v)$ by multiplying the appropriate rows and columns of $dF_1(v)$ and $dF_2(v)$. So

$$\begin{aligned} tr(df(v)) =& (1 - X_q'(\beta)\frac{L_q h}{s_\beta^3})(1 - X_p'(\alpha)\frac{L_P h}{r_\alpha^3}) + (-X_q'(\beta)\frac{L_q^2}{s_\beta^3})(-X_p'(\alpha)\frac{h^2}{r_\alpha^3}) \\ &+ (X_q'(\beta)\frac{h^2}{s_\beta^3})(X_p'(\alpha)\frac{L_P^2}{r_\alpha^3}) + (1 + X_q'(\beta)\frac{L_q h}{s_\beta^3})(1 + X_p'(\alpha)\frac{L_P h}{r_\alpha^3}) \\ =& 2 + X_p'(\alpha)X_q'(\beta)\left(\frac{2L_p L_q h^2 + L_q^2 h^2 + L_p^2 h^2}{r_\alpha^3 s_\beta^3}\right) \\ =& 2 + X_p'(\alpha)X_q'(\beta)\left(\frac{A^2 h^2}{r_\alpha^3 s_\beta^3}\right) \end{aligned}$$

Thus,

$$\lambda_1 = \frac{2 + X_p'(\alpha)X_q'(\beta)\left(\frac{A^2h^2}{r_\alpha^3 s_\beta^3}\right) + \sqrt{\left(2 + X_p'(\alpha)X_q'(\beta)\left(\frac{A^2h^2}{r_\alpha^3 s_\beta^3}\right)\right)^2 - 4}}{2}$$

and

$$\lambda_2 = \frac{2 + X_p'(\alpha)X_q'(\beta)\left(\frac{A^2h^2}{r_\alpha^3 s_\beta^3}\right) - \sqrt{\left(2 + X_p'(\alpha)X_q'(\beta)\left(\frac{A^2h^2}{r_\alpha^3 s_\beta^3}\right)\right)^2 - 4}}{2}$$

are the two eigenvalues of $df(v)$. Noticing that $X_p'(\alpha) < 0$, $X_q'(\beta) < 0$, $r_\alpha > 0$, and $s_\beta < 0$, one can see that $tr(df(v)) > 2$. Thus, remembering the product of the eigenvalues is equal to 1, we can now see the eigenvalues are distinct. Hence, one eigenvalue is strictly less than 1 and one is strictly greater than 1. Therefore, the Stable Manifold Theorem holds in all such cases and guarantees the existence of the shadow body in a neighborhood of v.

Further, we can then use the eigenvalues to compute the slope of the appropriate eigenvectors. The result that we achieved is that the slope of E_{λ_i}, the eigenvector corresponding to λ_i, can be computed by

$$\frac{\lambda_i - 1 + X_q'(\beta)(\frac{hL_q}{s_\beta^3}) + X_p'(\alpha)(\frac{L_p h}{r_\alpha^3}) - AX_p'(\alpha)X_q'(\beta)(\frac{h^2 L_q}{r_\alpha^3 s_\beta^3})}{X_p'(\alpha)(\frac{L_p^2}{r_\alpha^3}) - X_q'(\beta)(\frac{L_q^2}{s_\beta^3}) - AX_p'(\alpha)X_q'(\beta)(\frac{L_p L_q h}{r_\alpha^3 s_\beta^3})}.$$

The output corresponds to the slope of the stable or unstable manifold at v, depending on whether $|\lambda_i| < 1$ (stable manifold) or $|\lambda_i| > 1$ (unstable manifold).

5.2. **Visualizing the Stable Manifold.** At this point, we have computed the eigenvectors of the stable manifold and found them to match up with the tangent lines at the vertex. We have also found the eigenvectors for the unstable manifold. It would be nice to get a picture of what is actually happening with the construction of our shadow body to verify that it coincides with the behavior of our manifolds.

Figure 14 is the same picture as Figure 10.1 in Falconer [3] and describes how the fixed point is essentially the saddle point for the stable and unstable manifolds. When iterated by the function f, points along the stable manifold move toward the fixed point, points on the unstable manifold move directly away from the fixed point, and points elsewhere follow next to the stable manifold for a bit and then veer off along the same direction as the unstable manifold. If points are close to the stable manifold, but not quite on it, they will travel much closer to the fixed point before turning away.

Note: When observing the behavior of the stable and unstable manifolds, we no longer consider the X-ray functions to be piecewise. Instead, we let them take on negative values past the support rays because we are working in a neighborhood around the fixed point. The particular X-ray functions we have are only defined up to $\arccos(\sqrt{225-4}/15)$ *for* X_p *and* $\arccos(\sqrt{25-4}/5)$ *for* X_q *because of the radicals, but those values are still greater than the support rays.*

Figure 9 of the previous section revealed errors in the construction, and showed the tips of the body curving off in various directions. It was hard to tell if the direction of the curves had anything to do with the unstable manifold, but since the slopes for the left and right unstable manifolds were both negative (pointed up on the left but down on the right), and since the paths of the body continued upwards in both directions once past the support rays on both sides, it seemed unlikely. This turned out to be the case, but not because there was a problem with the construction. Rather, it was because in the construction, numerous points were getting moved with each iteration and the

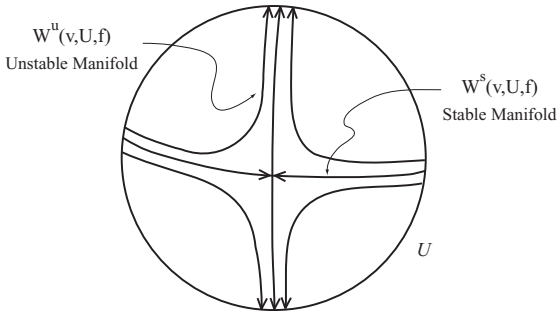

FIGURE 14. Stable and Unstable Manifolds in a Neighborhood of the Fixed Point v (Fig. 10.1 in Falconer [3]).

whole path was changing. But what the stable manifold really tells us about is the paths distinct points follow.

So we had a look at the journey of six points that started out near the base points, three points near the left base point and three near the right. The points on the left were iterated with the same function f that we have seen before, and the points on the right with a similar function that just started from source Q instead of P. Since there are two functions that operate from either side, there are two pairs of stable and unstable manifolds to consider. The points were at an initial height of 10^{-6} and at x-positions $7.431260, 7.431265, 7.431269$ and each of those values plus 1. As seen in Figure 15, the points starting on the left (in green) approach the vertex of the shadow body along the stable manifold, which is also the proper left tangent line, and then move away from the vertex along the steeper unstable manifold. The points starting on the right (in black) follow their own stable and unstable manifolds. The points 7.431265 and 8.431265 are actually so close to being the proper base points that they veer off in *opposite* directions near the fixed point, probably a result of the computer's computations being only approximate. To give an idea of the scale, this figure is about 0.03 units across while the body itself is 1 unit across.

6. CONVEXITY OF SHADOW BODY

6.1. **Local Convexity.** Now that we have determined local existence at the base points and vertices, we can continue our investigation of the potential shadow body by determining local convexity in those neighborhoods. In order to determine local convexity of a shadow body, it is helpful to use the curvature operator. Given a curve and a source from which the curve is defined, it is known that the curvature operator is positive if the curve is concave toward the source and negative if the curve is concave away from the source. Thus, it suffices to show that the curvature operator applied to r_p is negative and the curvature operator applied to R_p is positive (same for nearside and farside functions defined at Q).

We will begin by investigating the convexity at the baseline. Since we have determined the existence of the shadow body in a neighborhood of the baseline, we know that $r_p(\phi)$, $r_q(\psi)$, $R_p(\phi)$, $R_q(\psi)$ are defined for ϕ, ψ sufficiently small. We also have,

$$X_p(\phi) = R_p(\phi) - r_p(\phi) \text{ and } X_q(\psi) = R_q(\psi) - r_q(\psi).$$

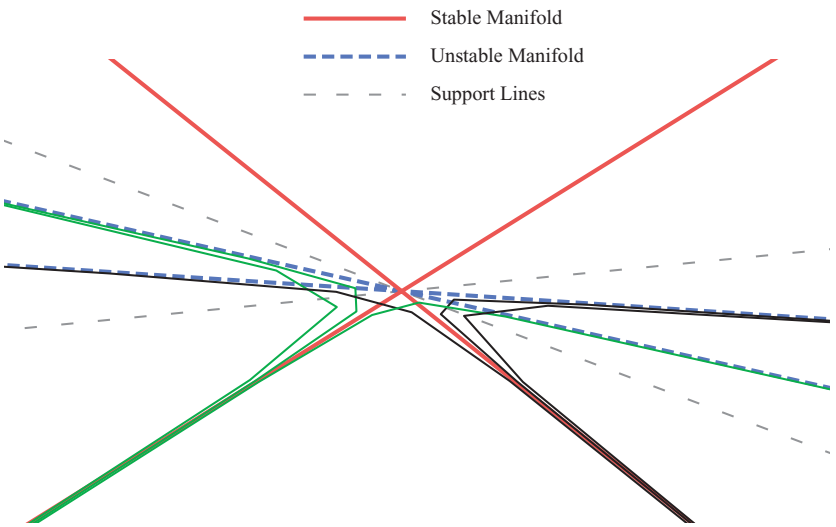

FIGURE 15. Paths of Iterated Points Following Stable and Unstable Manifolds

Using Lemma 3.8 on page 91 of [1], we have

$$\mathscr{K}X_p(0) = \mathscr{K}(R_p - r_p)(0) = \frac{X_p(0)}{R_p(0)}\mathscr{K}R_p(0) - \frac{X_p(0)}{r_p(0)}\mathscr{K}r_p(0) + 2R_p(0)r_p(0)\left[\frac{R_p'(0)}{R_p(0)} - \frac{r_p'(0)}{r_p(0)}\right]^2.$$

Similarly, computing at the source Q, we find that

$$\mathscr{K}X_q(0) = \mathscr{K}(R_q - r_q)(0) = \frac{X_q(0)}{R_q(0)}\mathscr{K}R_q(0) - \frac{X_q(0)}{r_q(0)}\mathscr{K}r_q(0) + 2R_q(0)r_q(0)\left[\frac{R_q'(0)}{R_q(0)} - \frac{r_q'(0)}{r_q(0)}\right]^2.$$

What seems to be two equations with four unknowns, can be further simplified by using the previously mentioned fact that the curvature operator of a function is related to the signed curvature, and the signed curvature is invariant of parameterization.

Thus, we have

$$\frac{\mathscr{K}R_p}{((R_p)^2 + (R_p')^2)^{3/2}} = \kappa R_p = \kappa r_q = \frac{\mathscr{K}r_q}{((r_q)^2 + (r_q')^2)^{3/2}}.$$

Similarly, we have

$$\frac{\mathscr{K}r_p}{((r_p)^2 + (r_p')^2)^{3/2}} = \kappa r_p = \kappa R_q = \frac{\mathscr{K}R_q}{((R_q)^2 + (R_q')^2)^{3/2}}.$$

We know from [1], that $r_p'(\phi) = r_p\cot(\eta_\phi - \phi)$ and $R_p'(\phi) = R_p\cot(\omega_\phi - \phi)$ where μ is the angle of inclination of the line tangent to the body at the point $(r_p(\phi), \phi)$ and ω is the angle of inclination of the line tangent to the body at the point $(R_p(\phi), \phi)$ (similar for Q). We want to solve this system at the baseline where ϕ and ψ are equal to 0. We know from [7] that η_ϕ and ω_ϕ can be computed at the baseline. Thus, we have a system of two equations with two unknowns and we can solve for local concavity.

In our particular case, the problem is simplified by the fact that we know our body is symmetric

over the x-axis. This implies that the tangent lines at the base points are vertical, thus, the nearside and farside derivatives from both sources are equal to zero. Therefore, we have the system

$$\begin{pmatrix} \frac{X_p(0)}{R_p(0)} & \frac{-X_p(0)}{r_p(0)} \\ \frac{-X_q(0)(r_q(0))^3}{R_q(0)(R_p(0))^3} & \frac{X_q(0)(R_q(0))^3}{R_q(0)(r_p(0))^3} \end{pmatrix} \begin{pmatrix} \mathscr{K}R_p(0) \\ \mathscr{K}r_p(0) \end{pmatrix} = \begin{pmatrix} \mathscr{K}X_p(0) \\ \mathscr{K}X_q(0) \end{pmatrix}.$$

This system can be solved using basic linear algebra. Computing this system for our particular example and making the appropriate conversion, we achieved baseline curvature values of -1.3191 and 1.5426 for the nearside and farside (with respect to P) of our potential shadow body. Therefore, the potential shadow body is convex in a neighborhood of the baseline.

The situation at the vertices is a little more cumbersome. Noticing that the X-ray data at the vertices is zero, the previous method will not work because the things we need to solve for end up canceling out. Using similar methods, one must be wary of dividing by the X-ray data. We deduced the following method in order to solve the problem.

Theorem 6.1. *Let $X_p(\phi)$ be a directed x-ray of a body defined at a source P. Let α be a support angle of the x-ray function. Then*

$$\mathscr{K}R_p(\alpha) - \mathscr{K}r_p(\alpha) = -r_p(\alpha)X_p''(\alpha) + 4X_p'(\alpha)r_p'(\alpha) - 2(X_p'(\alpha))^2.$$

Proof. Utilizing Lemma 3.8 from [1], we get

$$\mathscr{K}X_p = \mathscr{K}(R_p - r_p) = \frac{X_p}{R_p}\mathscr{K}R_p - \frac{X_p}{r_p}\mathscr{K}r_p + 2r_pR_p\left[\frac{R_p'}{R_p} - \frac{r_p'}{r_p}\right]^2.$$

Moving things around, we find that

$$\frac{\mathscr{K}R_p}{R_p} - \frac{\mathscr{K}r_p}{r_p} = \frac{\mathscr{K}X_p}{X_p} - \frac{2r_pR_p}{X_p}\left[\frac{R_p'}{R_p} - \frac{r_p'}{r_p}\right]^2.$$

Noticing that $R_p = r_p + X_p$ and $R_p' = r_p' + X_p'$, we see that

$$\begin{aligned} \frac{2r_pR_p}{X_p}\left[\frac{R_p'}{R_p} - \frac{r_p'}{r_p}\right]^2 &= \frac{2r_pR_p}{X_p}\left[\frac{r_p' + X_p'}{r_p + X_p} - \frac{r_p'}{r_p}\right]^2 \\ &= \frac{2r_pR_p}{X_p}\left[\frac{r_pX_p' - r_p'X_p}{r_pR_p}\right]^2 \\ &= \frac{2}{X_pr_pR_p}\left[r_pX_p' - r_p'X_p\right]^2 \\ &= \frac{2r_pX_p}{R_p}\left[\frac{X_p'}{X_p} - \frac{r_p'}{r_p}\right]^2 \end{aligned}$$

Recognizing that

$$\frac{r_p}{R_p} = \frac{r_p}{r_p + X_p} = 1 - \frac{X_p}{r_p + X_p} = 1 - \frac{X_p}{R_p},$$

we can continue to get

$$\frac{2r_pR_p}{X_p}\left[\frac{R_p'}{R_p}-\frac{r_p'}{r_p}\right]^2=2X_p\left[\frac{X_p'}{X_p}-\frac{r_p'}{r_p}\right]^2-\frac{2(X_p)^2}{R_p}\left[\frac{X_p'}{X_p}-\frac{r_p'}{r_p}\right]^2.$$

Substituting back into our original equation, we see that

$$\frac{\mathscr{K}R_p}{R_p}-\frac{\mathscr{K}r_p}{r_p}=\frac{\mathscr{K}X_p}{X_p}-2X_p\left[\frac{X_p'}{X_p}-\frac{r_p'}{r_p}\right]^2+\frac{2(X_p)^2}{R_p}\left[\frac{X_p'}{X_p}-\frac{r_p'}{r_p}\right]^2.$$

We can now see that

$$\begin{aligned}\frac{\mathscr{K}X_p}{X_p}-2X_p\left[\frac{X_p'}{X_p}-\frac{r_p'}{r_p}\right]^2&=\frac{(X_p)^2+2(X_p')^2-X_pX_p''}{X_p}-2X_p\left[\left(\frac{X_p'}{X_p}\right)^2-2\frac{X_p'}{X_p}\frac{r_p'}{r_p}+\left(\frac{r_p'}{r_p}\right)^2\right]\\&=X_p-X_p''+4X_p'\frac{r_p'}{r_p}-2X_p\left(\frac{r_p'}{r_p}\right)^2.\end{aligned}$$

Substituting back in and squaring the last piece, we finally get

$$\frac{\mathscr{K}R_p}{R_p}-\frac{\mathscr{K}r_p}{r_p}=X_p-X_p''+4X_p'\frac{r_p'}{r_p}-2X_p\left(\frac{r_p'}{r_p}\right)^2+\frac{2(X_P)^2}{R_p}\left[\left(\frac{X_p'}{X_p}\right)^2-2\frac{r_p'}{r_p}\frac{X_p'}{X_p}+\left(\frac{r_p'}{r_p}\right)^2\right].$$

Now if we let $\phi\to\alpha$, then $X_p\downarrow 0$, $r_p(\phi)\to r_p(\alpha)$, $R_p(\phi)\to R_p(\alpha)$, and $r_p(\alpha)=R_p(\alpha)$. Thus,

$$\frac{(\mathscr{K}R_p)(\alpha)}{r_p(\alpha)}-\frac{(\mathscr{K}r_p)(\alpha)}{r_p(\alpha)}=-X_p''(\alpha)+4X_p'(\alpha)\frac{r_p'(\alpha)}{r_p(\alpha)}-2\frac{(X_p'(\alpha))^2}{r_p(\alpha)}.$$

And finally, we have

$$\mathscr{K}R_p(\alpha)-\mathscr{K}r_p(\alpha)=-r_p(\alpha)X_p''(\alpha)+4X_p'(\alpha)r_p'(\alpha)-2(X_p'(\alpha))^2.$$

□

Similarly, we can obtain the same equality from the source Q, using the support angle β. Thus,

$$\mathscr{K}R_q(\beta)-\mathscr{K}r_q(\beta)=-r_q(\beta)X_q''(\beta)+4X_q'(\beta)r_q'(\beta)-2(X_q'(\beta))^2.$$

Notice that we have simply reduced the problem to two equations in two unknowns, since we can compute everything on the right side of the equality using methods previously discussed. Thus, utilizing the fact that the curvature operator is related to the signed curvature and that signed curvature is independent of parameterization, we can come up with the following system.

$$\begin{pmatrix}1 & -1\\ -\left(\frac{(r_q(\beta))^2+(r_q'(\beta))^2}{(r_p(\alpha))^2+(R_p'(\alpha))^2}\right)^{3/2} & \left(\frac{(r_q(\beta))^2+(R_q'(\beta))^2}{(r_p(\alpha))^2+(r_p'(\alpha))^2}\right)^{3/2}\end{pmatrix}\begin{pmatrix}\mathscr{K}R_p(0)\\ \mathscr{K}r_p(0)\end{pmatrix}$$
$$=\begin{pmatrix}-r_p(\alpha)X_p''(\alpha)+4X_p'(\alpha)r_p'(\alpha)-2(X_p'(\alpha))^2\\ -r_q(\beta)X_q''(\beta)+4X_q'(\beta)r_q'(\beta)-2(X_q'(\beta))^2\end{pmatrix}.$$

Again, this system can be solved using linear algebra methods. We used this approach with our particular example, and achieved signed curvature values of $-.39368$ and 0.11352 for the nearside and farside with respect to P. Thus, we have established that our potential shadow body is convex

in a neighborhood of the top vertex. Symmetry across the x-axis also insures convexity at the bottom vertex.

6.2. **Convexity Of the Computerized Construction.** Another test we ran on the constructions done in Matlab was that of convexity. Using the quadratic form Q from [1], we are able to apply Q to three points at a time on either side of the body. If each group of three points has the proper convexity, then the whole side has the right convexity. If there is one group of points where Q yields the wrong sign, then the whole body cannot be convex.

For construction from the bottom up, the body would have the right convexity right up until the very top when approximation errors kicked in. For construction from the bottom down, the body would usually have the right convexity everywhere. The only time this was not the case was when too many iterations caused points to cluster near the baseline, and approximation errors affected their convexity.

7. Proposed Construction of Shadow Body

When discussing the Stable Manifold Theorem and local existence, we introduced a function f. We will now use that function to develop a method for constructing our shadow body. This method is incomplete and we will discuss the specific uncertainties as they come up. The purpose of including this section is that we feel this method simplifies the problem.

We have already established that the stable manifold of f near v is a differentiable curve. Thus, if we let f^n signify the n^{th} iteration of f, we know that there exists a differentiable curve, C, in the neighborhood of v where $\lim_{n\to\infty} f^n(x,y) = v$ for every $(x,y) \in C$. Therefore, we have achieved existence of the nearside function of the shadow body (w.r.t P) in a neighborhood of v. We also know the slope of the tangent to C at v, as stated previously. Let $C = C_p(\phi)$ be defined (in an appropriately small interval less than or equal to α) using polar coordinates from P and similarly let $C = C_q(\psi)$ be defined using polar coordinates from Q. Define $g : D \to \mathbb{R}^2$ as $g = f^{-1}$. It is clear that g is continuous. Let r denote the set of points in D that are in the global stable manifold of v with respect to f.

We can now build a sequence of differentiable curves and show that they converge to r on the interval $(0,\alpha]$, thereby showing that r is a differentiable curve. Let $\phi_1 < \alpha$ so that the ray emanating from P with angle of inclination ϕ_1 intersects C. Define $r_1 : (0,\alpha] \to \mathbb{R}$ by

$$r_1(\phi) = \begin{cases} C(\phi) & \text{if } \phi \geq \phi_1 \\ \frac{C(\phi_1)}{\sec(\phi_1)} \sec\phi & \text{else.} \end{cases}$$

Then r_1 is a continuous function on $(0,\alpha]$. See Figure 16 We can then compute $g \circ r_1$ and let it be represented in polar coordinates centered at P by r_2^*. Let ϕ_2 be the angle of inclination of the line segment from P to $g(r_1(\phi_1))$. Define $r_2 : (0,\alpha] \to \mathbb{R}$ by

$$r_2(\phi) = \begin{cases} r_2^*(\phi) & \text{if } \phi \geq \phi_2 \\ \frac{r_2^*(\phi_2)}{\sec(\phi_1)} \sec\phi & \text{else.} \end{cases}$$

Recursively build the sequence $(r_n)_n$ of continuous functions defined on $(0,\alpha]$ by defining $r_n : (0,\alpha] \to \mathbb{R}$ by

$$r_n(\phi) = \begin{cases} r_n^*(\phi) & \text{if } \phi \geq \phi_n \\ \frac{r_n^*(\phi_n)}{\sec(\phi_1)} \sec\phi & \text{else} \end{cases}$$

where r_n^* is the polar representation (centered at P) of $g^{n-1}(r_1)$, and ϕ_n is the angle of inclination of the line segment connecting P to $g^{n-1}(r_1(\phi_1))$.

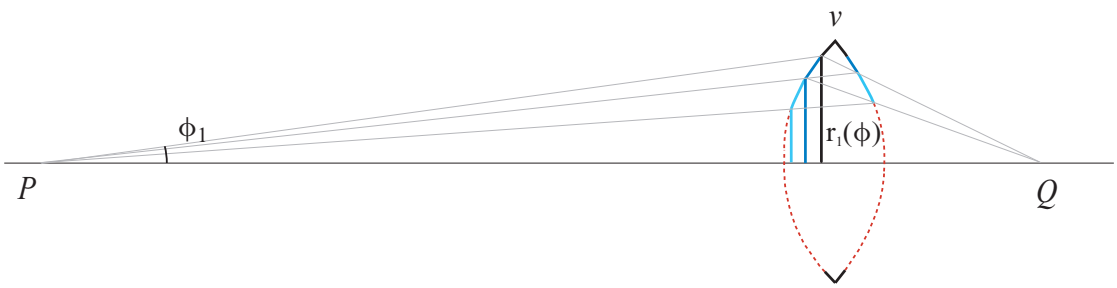

FIGURE 16. The piecewise functions $r_1(\phi)$, $r_2(\phi)$, $r_3(\phi)$ converging to r.

Notice that $r = r_n$ when the domain is restricted to $[\phi_n, \alpha]$.

Question: This method makes the assumption that it is possible to define each iteration as a function defined using polar coordinates from P. We have been unable to show this explicitly and it needs more investigation.

Conjecture 7.1. *r is a differentiable curve on the domain $(0, \alpha)$.*

Proof. We can show this by proving that $(r_n)_n$ converges to r on $[\varepsilon, \alpha]$ for any $\varepsilon > 0$ and also noting that the resulting curve is differentiable. Let $\varepsilon > 0$ be given. It's clear from the way we defined f that the characteristic function $\lim_{n\to\infty} \pi_2(g^n(x,y)) = 0$ for any $(x,y) \in D$. Thus, $\lim_{n\to\infty} \pi_2(g^n(r_1(\phi_1)) = 0$ and so $\lim_{n\to\infty} (\phi_n)_n = 0$. Let $N \in \mathbb{X}^+$ so that $\phi_n < \varepsilon$. Then for all $n \geq N$, $r_n = r$ on $[\varepsilon, \alpha]$. Thus, for each $\varepsilon > 0$, there exists an N so that $r_N(\phi) = r(\phi)$ for all $\phi \in (\varepsilon, \alpha]$. Since each r_n is a finite differentiable iteration of a smooth curve, r is differentiable on (ε, α).

□

Question: What happens near the baseline? Although we know that our resulting curve will be differentiable, we are not sure whether it will behave near the baseline. Essentially, it needs to be shown that r will converge to a point on the baseline, and not bounce back and forth as it approaches the baseline.

Successfully answering the two questions in the section would ensure that there exists a body, star-shaped at P, with the same point X-rays as the example we referred to in the introduction. We would simply need to reflect it over the x-axis and it's easy to show that it has the same point x-rays. This would be a major success in the field, but it would be left to show that the body in question is convex.

8. Conclusion

One final test was to go through the process of X-raying the constructed shadow body to make sure the data actually matched up with the initially defined X-ray function. The construction algorithms we implemented built the left side of the shadow body and then defined the right side of the shadow body as each point on the left side plus the x-ray data from source P. While this guaranteed that the x-rays of the constructed body from source P would be correct, it did not guarantee that the same would be true from source Q. So, for numerous angles from Q, we took the line emanating from Q at each angle (measured clockwise) and used Matlab to find the intersection of that line with the line segments making up the left and the right sides of the constructed body. Each side of the body was stored as an array of discrete points, so each side was essentially a combination of a bunch of piecewise linear functions. Matlab has a function called `polyxpoly` that makes it very easy to find the intersection of a line with a bunch of line segments. See Figure 17 for a picture of a few X-ray 'beams' from Q intersecting the object. Only six angles are shown here for simplicity, but we have computed the x-ray data for up to 3000 angles. If the line hits both sides of the object, then the X-ray data for that particular angle is simply the distance between the two points of intersection.

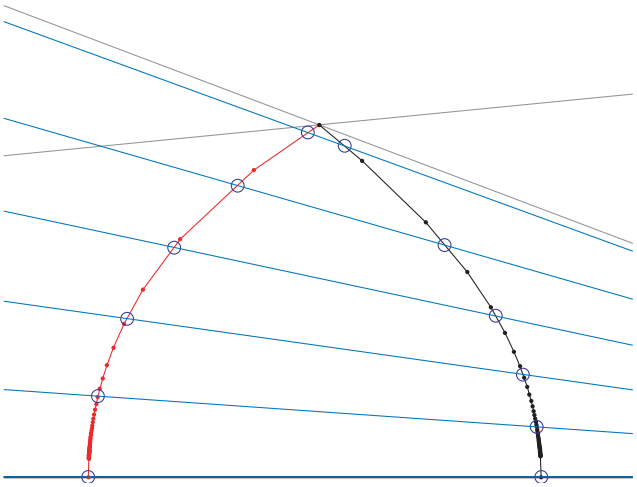

FIGURE 17. X-Rays From Source Q Intersecting Constructed Body

One particular reconstruction done from the top down with an initial angle of 10^{-10} radians, 19 iterations, and 110 points, when the generated X-ray data from Q was compared to the original X-ray data, the maximum error between the two functions was 0.0021. When 310 points were used with the same initial angle and number of iterations, the maximum error went down to 2.9644×10^{-4}. Adding points while keeping the size of the initial neighborhood the same had the effect of smoothing out the curve of the constructed body. 510 points yielded a maximum difference of 1.1460×10^{-4}. When the number of iterations was reduced to 17, which put less of a force on each point to move toward the baseline, and when 650 points were used in total, the maximum error went all the way down to 4.2593×10^{-6}. Once again, this is further evidence that we are in good shape with our construction algorithm and that the approximate constructed body is very close to the shadow body we are looking for.

Throughout this study, we have made interesting observations related to the existence of two bodies with equal point X-rays at two sources. Given a convex planar body and two sources where the line between the sources passes through the body, we have shown results that explicitly state when there is a possibility for a second body with the same X-rays to exist, and when the two sources are sufficient in uniquely defining one convex body. This also leads to a consistency criteria that must be met by two point X-ray functions of any convex body. We have investigated one particular example of a convex body and utilized the Stable Manifold Theorem to show local existence of a second body at various points. We have shown that this method of showing local existence works in the general case, as well. Additionally, we have shown convexity in each neighborhood where we have existence of a shadow body.

Computer constructions have played a key role in our investigation, and have given us a lot of evidence to persuade us that the existence of a convex shadow body is, indeed, very probable. We have not actually been able to prove existence, but we feel that further investigation could very likely lead to proving the that two convex bodies with equal point X-rays at two sources exist. The key to solving this problem is likely to be to gain a better understanding of how the stable manifold behaves globally, and analyze the behavior of the various functions which give rise to the stable manifold.

REFERENCES

[1] W. Black, J. Kimble, D. Koop, D.C. Solmon, *Functions that are the Directed X-Ray of a Planar Convex Body.* Rend. Istit. Mat. Univ. Trieste. Vol. XXXV, 81-115 (2003).
[2] M. Dartmann, *Rekonstrucktion Konvexer, Homogener Gebiete aus Wenigen Punktquellen*, Diplomarbeit. U. Munster, Germany. (1991)
[3] K.J. Falconer, Hammer's X-Ray Problem and the Stable Manifold Theorem. *J. London Math. Soc.* (2), **28** (1983), 149-160.
[4] K.J. Falconer, X-ray Problems for Point Sources. *Proc. London Math. Soc.* (3) **46** (1983), 242-262.
[5] R.J. Gardner, *Geometric Tomography.* Encyclopedia of Mathematics and its Applications, vol. 58. Cambridge University Press, 1995.
[6] R.J. Gardner, *Symmetrals and X-rays of Planar Convex Bodies*, Arch. Math. 41, 1983, 183-189.
[7] J. Seifken, L. Spargo. *An Algorithm for Reconstruction of a Convex Body From Two Point Sources*, Proceedings from 2005 REU Program in Mathematics at Oregon State University
[8] A. Volcic. *A Three Point Solution to Hammer's X-ray Problem*, J. London Math. Soc. (2) 40, 1989, 171-178.

UNIVERSITY OF NORTHERN IOWA
E-mail address: dross@uni.edu

UNIVERSITY OF CALIFORNIA, SANTA CRUZ
E-mail address: ktuite@ucsc.edu